

***In-situ* grown NiCo bimetal anchored on porous straw-derived biochar composites with boosted microwave absorption properties**

Yuanyuan Zhou, Zhongyi Bai, Xiangyang Yang, Wei Liu, Bingbing Fan, Zhikai Yan, and Xiaoqin Guo

Cite this article as:

Yuanyuan Zhou, Zhongyi Bai, Xiangyang Yang, Wei Liu, Bingbing Fan, Zhikai Yan, and Xiaoqin Guo, *In-situ* grown NiCo bimetal anchored on porous straw-derived biochar composites with boosted microwave absorption properties, *Int. J. Miner. Metall. Mater.*, 30(2023), No. 3, pp. 515-524. <https://doi.org/10.1007/s12613-022-2496-2>

View the article online at [SpringerLink](#) or [IJMMM Webpage](#).

Articles you may be interested in

Peng Zhou, Jun-hong Chen, Meng Liu, Peng Jiang, Bin Li, and Xin-mei Hou, [Microwave absorption properties of SiC@SiO₂@Fe₃O₄ hybrids in the 2-18 GHz range](#), *Int. J. Miner. Metall. Mater.*, 24(2017), No. 7, pp. 804-813. <https://doi.org/10.1007/s12613-017-1464-8>

Yang He, Jian Liu, Jian-hua Liu, Chun-lin Chen, and Chang-lin Zhuang, [Carbothermal reduction characteristics of oxidized Mn ore through conventional heating and microwave heating](#), *Int. J. Miner. Metall. Mater.*, 28(2021), No. 2, pp. 221-230. <https://doi.org/10.1007/s12613-020-2037-9>

Peng Liu, Li-bo Zhang, Bing-guo Liu, Guang-jun He, Jin-hui Peng, and Meng-yang Huang, [Determination of dielectric properties of titanium carbide fabricated by microwave synthesis with Ti-bearing blast furnace slag](#), *Int. J. Miner. Metall. Mater.*, 28(2021), No. 1, pp. 88-97. <https://doi.org/10.1007/s12613-020-1985-4>

Ying-jun Qiao, Huan Zhang, Yu-xin Hu, Wan-peng Li, Wen-jing Liu, Hui-ming Shang, Mei-zhen Qu, Gong-chang Peng, and Zheng-wei Xie, [A chain-like compound of Si@CNT nanostructures and MOF-derived porous carbon as an anode for Li-ion batteries](#), *Int. J. Miner. Metall. Mater.*, 28(2021), No. 10, pp. 1611-1620. <https://doi.org/10.1007/s12613-021-2266-6>

Subhmit K. Roy, Deepak Nayak, Nilima Dash, Nikhil Dhawan, and Swagat S. Rath, [Microwave-assisted reduction roasting–magnetic separation studies of two mineralogically different low-grade iron ores](#), *Int. J. Miner. Metall. Mater.*, 27(2020), No. 11, pp. 1449-1461. <https://doi.org/10.1007/s12613-020-1992-5>

Ping-hu Chen, Yun Zhang, Rui-qing Li, Yan-xing Liu, and Song-sheng Zeng, [Influence of carbon-partitioning treatment on the microstructure, mechanical properties and wear resistance of *in situ* VCp-reinforced Fe-matrix composite](#), *Int. J. Miner. Metall. Mater.*, 27(2020), No. 1, pp. 100-111. <https://doi.org/10.1007/s12613-019-1909-3>



IJMMM WeChat



QQ author group

***In-situ* grown NiCo bimetal anchored on porous straw-derived biochar composites with boosted microwave absorption properties**

Yuanyuan Zhou¹, Zhongyi Bai², Xiangyang Yang¹, Wei Liu¹, Bingbing Fan³,✉, Zhikai Yan¹, and Xiaoqin Guo¹,✉

1) Henan Key Laboratory of Aeronautical Materials and Application Technology, School of Material Science and Engineering, Zhengzhou University of Aeronautics, Zhengzhou 450046, China

2) School of Chemical & Environmental Engineering, China University of Mining & Technology (Beijing), Beijing 100083, China

3) School of Material Science and Engineering, Zhengzhou University, Zhengzhou 450001, China

(Received: 29 January 2022; revised: 12 April 2022; accepted: 14 April 2022)

Abstract: With the gradually increasing protection awareness about electromagnetic pollution, the demand for absorbing materials with renewability and environmental friendliness has attracted widespread attention. In this work, composites consisting of straw-derived biochar combined with NiCo alloy were successfully fabricated through high-temperature carbonization and subsequent hydrothermal reaction. The electromagnetic parameters of the porous biocarbon/NiCo composites can be effectively modified by altering their NiCo content, and their improved absorbing performance can be attributed to the synergy effect of magnetic–dielectric characteristics. An exceptional reflection loss of -27.0 dB at 2.2 mm thickness and an effective absorption bandwidth of 4.4 GHz (11.7–16.1 GHz) were achieved. These results revealed that the porous biocarbon/NiCo composites could be used as a new generation absorbing material because of their low density, light weight, excellent conductivity, and strong absorption.

Keywords: straw-derived biochar; microwave absorption; interfacial polarization; magnetic loss; bimetallic NiCo; impedance matching.

1. Introduction

The rapid progress of electronic technology has gradually produced a series of problems, such as electromagnetic (EM) radiation and electromagnetic interference (EMI) [1–4]. Exploring excellent microwave absorption materials is urgently warranted to resolve these serious problems. The easiest and most effective method is to find a material with high conductivity and improve its absorbing performance by promoting strong conductive loss and dielectric loss [5–8].

Highly conductive materials mainly include metals [9–13] (Fe, Co, Ni, Cu, and Ag), carbon materials [14–18] (graphene, graphite, carbon black, carbon fiber, and carbon nanotubes), and conductive polymers [19–21] (polyacetylene, polypyrrole, and polyaniline). Among these, carbon materials have aroused significant enthusiasm due to their merits of low density, light weight, high aspect ratio and conductivity, good dielectric properties, low specific gravity, and strong chemical stability. Despite their many advantages, carbon materials still have the problems of complicated preparation and high economic cost. Therefore, the development of a novel method to fabricate carbon materials will be of scientific significance.

Biomass is an attractive renewable resource, and its utiliz-

ation and development exhibit the sustainable cycle feature. It is a natural carrier of carbon elements and has a great potential to be converted into functional carbon materials. In general, biomass is abundant in nature, including forests, agriculture, aquatic vegetation, and crustaceans. Moreover, biomass waste has become one of the largest pollutants in the world, and its utilization will help protect resources and the environment. Many biomass carbon materials have been used as absorbing materials. For example, Aslam *et al.* [22] selected wheat straw as a carbon source and controlled its KOH content to modify the microstructure of the generated 3D foam-like biocarbon with a minimal reflection loss (RL_{\min}) of -37 dB and an effective absorption band (EAB) of 8.8 GHz (7.2–16 GHz). Yan's group [23] proposed a cellulose-derived carbon aerogel that was obtained through carbonization at a low temperature of about 550°C for 2 h and showed exceptional RL_{\min} of -43.6 dB and EAB of 7.42 GHz. Zhao *et al.* [24] prepared porous skeleton carbon media by employing wheat flour as the biomass carbon source, and the carbon material showed an exceptional absorbing ability with an RL_{\min} of -51 dB. Sun *et al.* [25] fabricated a hierarchical carbonized waxberry, and the natural radial-gradient structure endowed the biomass with strong polarization loss because of the gradient dielectric property.

✉ Corresponding authors: Bingbing Fan E-mail: fanbingbing@zzu.edu.cn; Xiaoqin Guo E-mail: guoxq@zua.edu.cn

However, the EM wave absorption property of a single carbon component is seriously restrained by poor impedance matching. To alleviate the impedance mismatch caused by highly conductive carbon materials, Gou's group [26] synthesized biocarbon composites by using $\text{FeCl}_3 \cdot 6\text{H}_2\text{O}$ as the magnetic raw material and found that the formed magnetic nanoparticles are beneficial for the improvement of magnetic loss. Studies have also been conducted on the absorbing performance of carbon-cotton/Co@nanoporous carbon [27], Ni/rice-derived porous carbon [28], biochar/(Fe,Ni) hybrid [29], bark-derived Co-doped porous carbon [30], and ferrite/biocarbon [31].

Owing to the double loss mechanism of magnetic composite materials, an enhanced microwave absorption capability can be obtained through the proper design and preparation of magnetic–dielectric composites. On the one hand, the dielectric carbon component acts as the center of electric polarization and prompts the reduction of eddy current loss caused by magnetic metals. On the other hand, the synergy effect of dielectric loss and magnetic loss favors a good impedance match. Herein, straw-derived biochar was obtained by acid washing and subsequent high-temperature annealing. The as-fabricated biocarbon composites anchored with magnetic NiCo were synthesized by the electrostatic assembly and *in-situ* reduction of Ni^{2+} and Co^{2+} ions. During carbonization and hydrothermal reaction, the addition of magnetic NiCo bimetal into biocarbon increased the interfacial polarization and impedance matching to improve the microwave absorption.

2. Experimental

2.1. Fabrication of biocarbon/NiCo composites

Straw-derived biochar was prepared as follows. Cleaned wheat straws were obtained through calcination, and the as-prepared wheat straw wastes were acidified by HF solution for 2 h and then washed with deionized water until the solution was neutralized. The mixture was then blended with KOH aqueous solution and dried at 70°C overnight. KOH was applied as an activation agent that contributes to the formation of micropores and defects in the biocarbon. The biocarbon product was then calcined at 1000°C under an inert atmosphere.

Straw-derived biocarbon/NiCo materials were fabricated by hydrothermal process. First, distilled water, hydrazine hydrate, biocarbon, $\text{CoCl}_2 \cdot 6\text{H}_2\text{O}$, and $\text{NiCl}_2 \cdot 6\text{H}_2\text{O}$ (equivalent molar ratio between Ni^{2+} and Co^{2+}) were combined and mixed evenly, transferred into a stainless-steel autoclave, and maintained at 180°C for 12 h. For convenience, the obtained biocarbon/NiCo materials prepared at 0.5, 1, and 2 mmol metal ions were labeled as C–NiCo-1, C–NiCo-2, and C–NiCo-3, respectively.

2.2. Material characterizations

The phase composition and surface chemical composition were measured by X-ray diffraction (XRD, Smart Lab, Ja-

pan) and X-ray photoelectron spectroscopy (XPS, Thermo Fisher ESCALAB 250Xi, USA), respectively. The microstructures were investigated by a scanning electron microscope (SEM, JSM-7001F, Japan) and a transmission electron microscope (TEM, JEOL, JEM-2100F, Japan). Specific surface area (S_{BET}) and pore structure were studied by analyzing N_2 adsorption–desorption isotherms. Functional groups and defect degree were investigated by a Fourier transform infrared spectroscope (FT-IR, Nicolet iS10, USA) and a Raman spectrometer (LabRAM HR Evolution, Japan), respectively. The EM parameters of the 30wt% biocarbon@NiCo/paraffin wax composites were measured by a vector network analyzer (Agilent N5234A, USA).

3. Results and discussion

3.1. Morphological and microstructural characterization of biocarbon/NiCo composites

The crystal structures of the straw-derived biocarbon/NiCo composites are shown in Fig. 1(a) and (b). The broad peak at 24° corresponded to amorphous carbon (Fig. 1(a)), indicating that biocarbon was successfully fabricated by calcining the wheat straws. The three diffraction peaks of the biocarbon/NiCo samples (Fig. 1(b)) located at 44.2°, 51.6°, and 76.0° were attributed to the (111), (200), and (220) crystal planes of face-centered cubic (FCC) metals, respectively. In addition, diffraction peaks were found between FCC Co (PDF No. 15-0806) and FCC Ni (PDF No. 04-0850) metals, indicating the formation of NiCo alloys [32].

The chemical states and surface elements of biocarbon/NiCo material were analyzed by XPS as shown in Fig. 1(c)–(f). According to the full spectra of the XPS survey (Fig. 1(c)), the biocarbon/NiCo composites consisted of C, O, Co, and Ni elements. In the high-resolution C 1s XPS spectra (Fig. 1(d)), the peaks located at binding energies of 284.8 and 285.4 eV confirmed the presence of C–C (sp^2 carbon atoms) and C–O bonds, respectively, which were obtained from carbonization and can be used as dipole polarization centers to cause polarization loss. In the Co 2p spectra (Fig. 1(e)), one typical peak located at 778.3 eV was attributed to the metallic state of Co. In addition, two peaks of 781.3 and 796.5 eV were associated with Co 2p_{3/2} and Co 2p_{1/2}, respectively, and accompanied by the shake-up satellite peaks (786.6 and 804.0 eV denoted as “Satellite”). This finding indicated the existence of minor oxidation on the Co surface. Similarly, the Ni 2p spectra (Fig. 1(f)) presented the typical peak for metallic Ni (853.0 eV). Ni oxidation was proven via the peaks of Ni 2p_{3/2} and Ni 2p_{1/2} (855.9 and 873.4 eV) and the two “Satellite” (861.7 and 879.6 eV). All these results confirmed the presence of NiCo metals and slight oxidation in the biocarbon composites [8].

Fig. 2 shows the SEM images of the biocarbon/NiCo products. A smooth surface and a few micropores could be observed in the pure straw-derived biochar, as shown in Fig. 2(a). Compared with that of pristine biocarbon, the surface of the straw-derived biochar composites gradually became

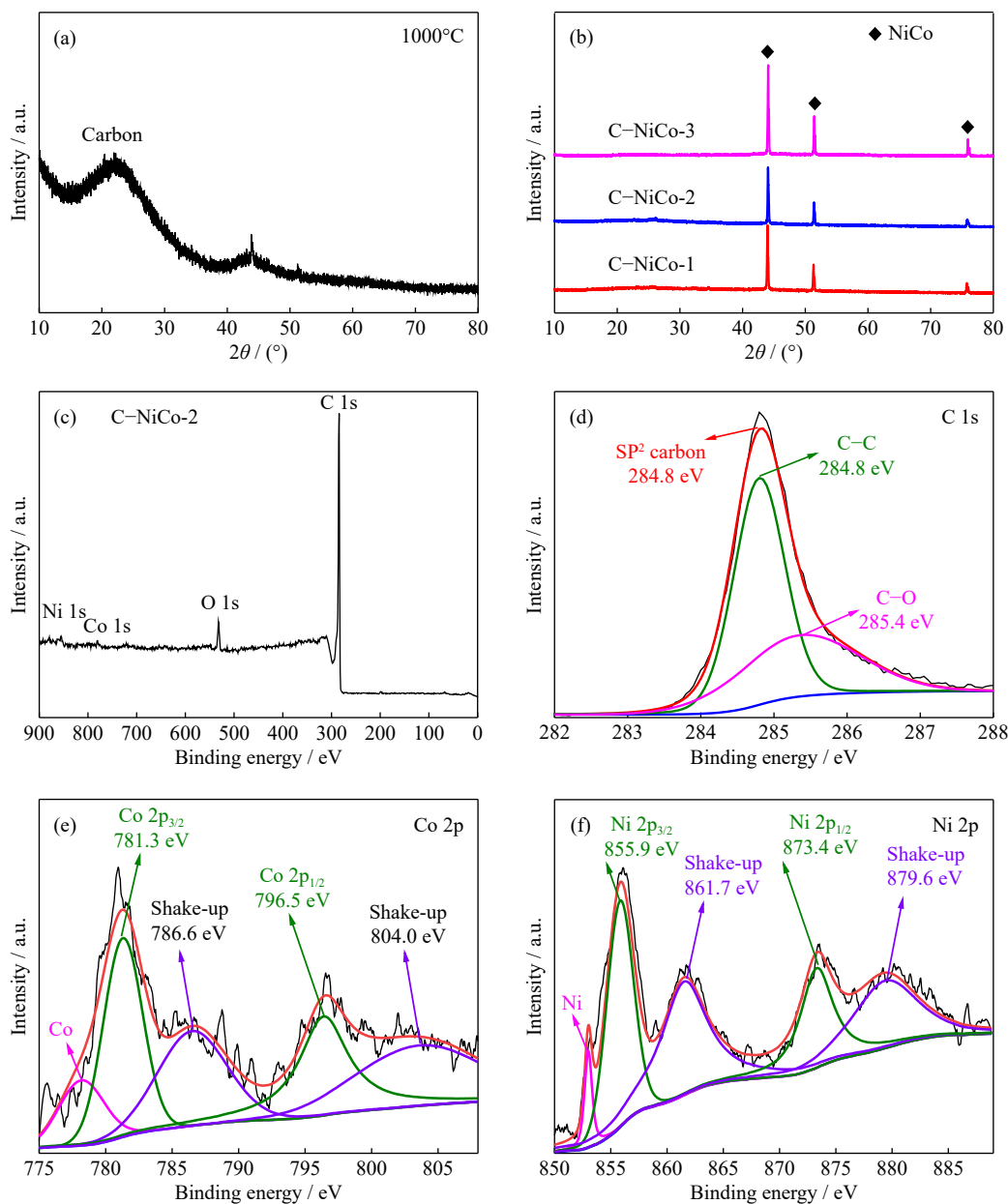


Fig. 1. XRD patterns of (a) pure biocarbon and (b) biocarbon/NiCo composites. XPS spectra of the biocarbon/NiCo sample: (c) survey scans, (d) C 1s, (e) Co 2p, and (f) Ni 2p.

rough due to the formation of numerous anchored NiCo nanoparticles. This finding revealed that the *in-situ* reduction of NiCo bimetal occurred during the hydrothermal reaction. The number of nanoparticles deposited on porous straw-derived biocarbon increased with the NiCo amount. Therefore, the addition of magnetic NiCo might be favorable for alleviating EM wave absorption.

The TEM and high-resolution TEM (HRTEM) images of straw-derived biocarbon/NiCo composites are shown in Fig. 3. As displayed in Fig. 3(a)–(c), the nanoparticles were evenly distributed in the amorphous biocarbon matrix, and almost no agglomeration was observed. Fig. 3(e) and (f) shows the HRTEM image of the biocarbon/NiCo sample. The NiCo particles were tightly anchored on the carbon even after intensive grinding. The interlayer spacing of the lattice fringes of the presented NiCo particle was 0.205 nm (Fig. 3

(f)), which is assigned to the (111) plane of face-centered cubic NiCo crystals. The considerably sharp ring-like features of the corresponding selected electron diffraction (SAED) pattern (Fig. 3(d)) suggest the polycrystalline nature of the as-prepared sample with clear (200) and (111) diffraction planes.

Fig. 4(a) shows the specific surface area and pore size of the three biocarbon/NiCo samples tested by N_2 adsorption–desorption isotherms. The hysteresis loop with type IV isotherm confirmed the formation of mesopores in the composites. The S_{BET} values of the C–NiCo-1, C–NiCo-2, and C–NiCo-3 samples (Fig. 4(b)) were 355.258, 400.003, and 357.185 m^2/g , respectively. In Fig. 4(b), the pore size of the three composites was mainly in the range of 0.2–5 nm, with an average of 2.59, 2.45, and 2.73 nm, indicating their mesoporous characteristics. Therefore, the large specific surface

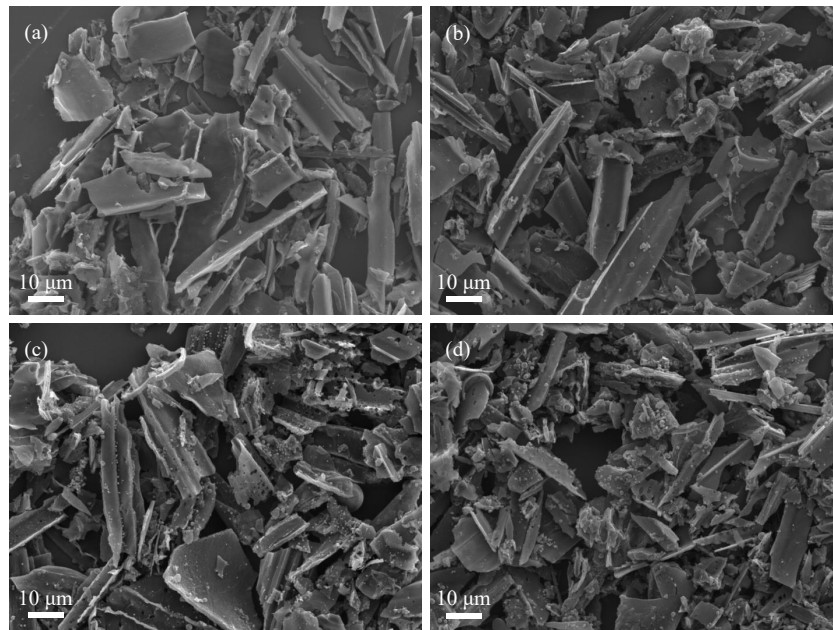


Fig. 2. SEM images of C/NiCo composites: (a) pure biocarbon, (b) C-NiCo-1, (c) C-NiCo-2, and (d) C-NiCo-3.

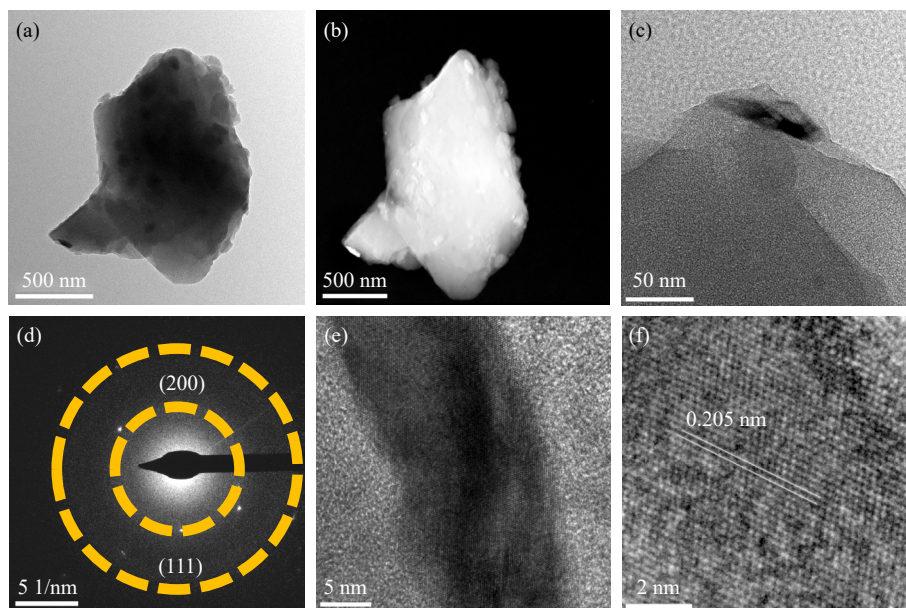


Fig. 3. TEM images with different resolution (a, c), dark-field TEM image (b), SAED patterns (d), and high-resolution TEM images (e, f) of biocarbon/NiCo composites under different resolution.

area and broad pore size distribution can cause intense interfacial polarizations, which is believed to boost EM absorption. Fig. 4(c) displays the Raman spectra for evaluating the carbon graphitization degree of these biocarbon/NiCo composites. The carbon component has two characteristic peaks, namely, D ($\sim 1350\text{ cm}^{-1}$) and G (1590 cm^{-1}) bands that are associated with the defects of the carbon atom lattice and the graphitized carbon atom, respectively. In addition, the value of I_D/I_G was used to evaluate the degree of graphitization of the carbon-based material, where I_D denotes the intensity of the D-peak and I_G denotes the intensity of the G-peak. As shown in Fig. 4(c), the I_D/I_G ratios of C-NiCo-1, C-NiCo-2, and C-NiCo-3 were 1.12, 1.24, and 1.03, respectively, which are slightly larger than that of pure biocarbon ($I_D/I_G = 1.02$). This finding indicated that the addition of NiCo alloy has minimal

effects on the graphitization degree. The slight change may originate from the catalytic graphitization effect of the NiCo alloy on local carbons [33]. The functional groups of the biocarbon/NiCo composites with different NiCo contents were characterized by FT-IR spectra (Fig. 4(d)). For the pure biocarbon, the characteristic absorption peaks of 3498 and 1629 cm^{-1} corresponded to the $-\text{OH}$ (hydroxyl) stretching vibration peak and the deformation vibration absorption peak of water molecules, respectively. The stretching vibration peaks at ~ 1384 and 1050 cm^{-1} were ascribed to the $-\text{C}-\text{O}$ and $-\text{C}-\text{OH}$, respectively. On the basis of the above results, the presence of the $-\text{OH}$ and $-\text{O}-\text{C}=\text{O}$ groups on the porous biocarbon surface confirmed that the straw-derived biochar could attract Ni^{2+} and Co^{2+} metal ions through electrostatic force.

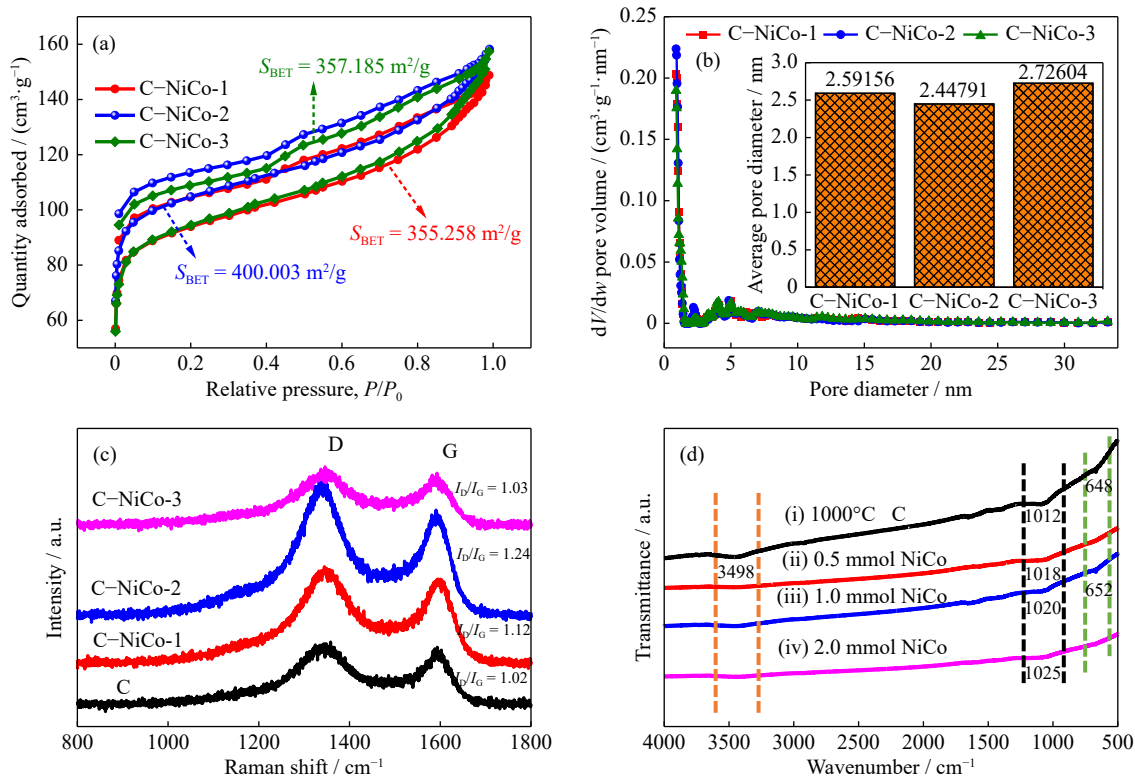


Fig. 4. Biocarbon/NiCo composites: (a) N_2 adsorption–desorption isotherm (standard temperature and pressure), (b) pore size distribution plots and average pore diameter in sert, (c) Raman spectra, and (d) FT-IR patterns.

3.2. Electromagnetic parameters of biocarbon/NiCo composites

Fig. 5 exhibits the measured EM parameters of the biocarbon/NiCo composites. The ϵ' values (Fig. 5(a)) for all the

samples decreased monotonously with the increasing frequency because of the hysteresis between the displacement current and the build-up potential [34–35]. The ϵ' values of different samples gradually decreased with the increasing amount of NiCo alloys. As shown in Fig. 5(b), the increasing

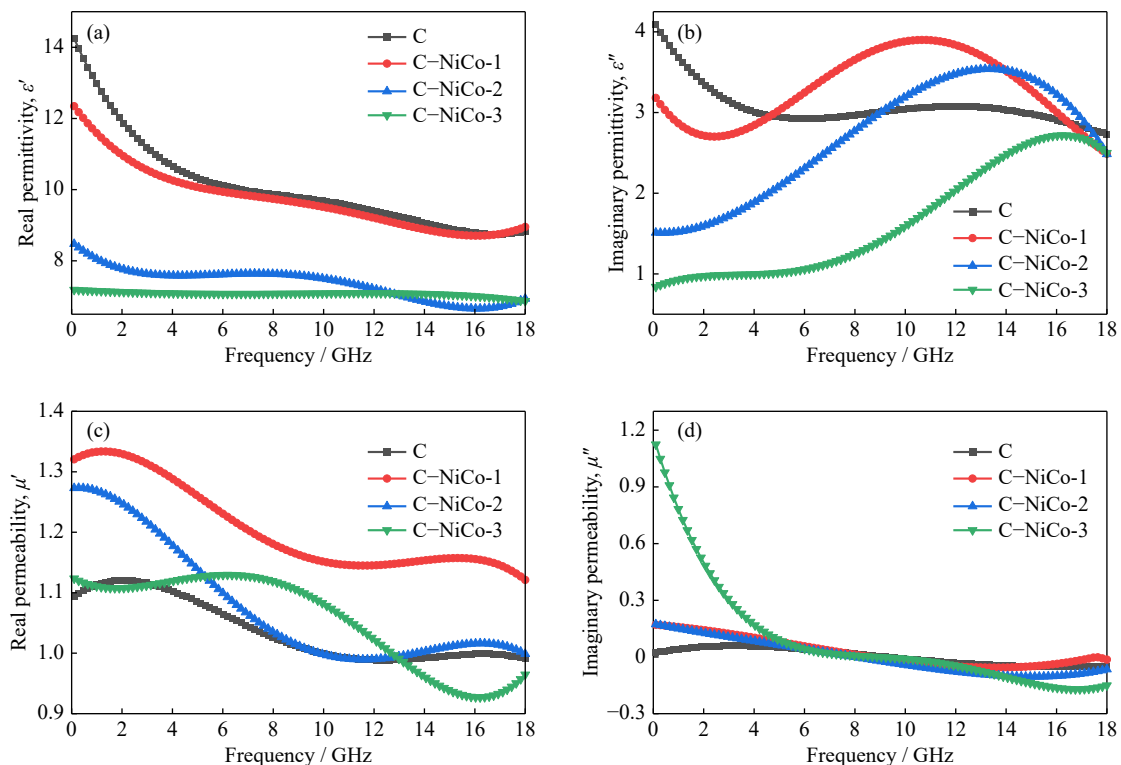


Fig. 5. EM parameters of the biocarbon/NiCo composites: (a) real permittivity ϵ' , (b) imaginary permittivity ϵ'' , (c) real permeability μ' , and (d) imaginary permeability μ'' .

ε'' value versus frequency could be attributed to the multiple polarization caused by numerous dipoles and the plentiful interfaces existing between the NiCo particles and the porous biocarbon. With further increase in the addition of NiCo alloys, the enhanced electrical conductivity resulted in high ε'' values and increased electron transfer efficiency according to free-space theory. Therefore, the dielectric constant of the biocarbon/NiCo materials could be adjusted by changing the contents of Ni^{2+} and Co^{2+} metal ions.

As shown in Fig. 5(c) and (d), the μ' and μ'' values of three biocarbon/NiCo samples showed a decreasing trend within the measured frequency, and all biocarbon/NiCo samples showed low μ' and μ'' values in the high frequency. This finding indicates that the magnetic loss of biocarbon/NiCo materials might be inhibited in the high frequency region due to Snoek's limitation [36–38]. Compared with pure biocarbon, the biocarbon/NiCo composites have larger μ'' values in the low frequency that were indicative of magnetic loss due to the addition of NiCo alloys. Furthermore, the negative μ'' values in 10–18 GHz reveals that magnetic energy radiated out from the biocarbon/NiCo due to the motion of charges; this finding is related to the alternating EM field based on the Maxwell equations.

In general, the microwave energy dissipated in an applied electric field is attributed to conductivity and polarization loss. However, the use of materials with low amounts of the biocarbon/NiCo can suppress the formation of conductive networks in paraffin wax-based composites to a certain degree (30wt%). Therefore, the ohmic loss is not the main contributor to dielectric loss [39]. Owing to the vast contacting

sites among porous biocarbon and NiCo alloys, a great number of dipolar pairs would accumulate in their interfaces and result in interfacial polarization loss. The relationship between the real and imaginary parts of the dielectric constant was drawn, as shown in Fig. 6, to further analyze the polarization relaxation process. This relationship can be expressed by the Debye dipolar polarization in the following equation of cole–cole curve [40–41]:

$$\left(\varepsilon' - \frac{\varepsilon_s + \varepsilon_\infty}{2}\right)^2 + (\varepsilon'')^2 = \left(\frac{\varepsilon_s - \varepsilon_\infty}{2}\right)^2 \quad (1)$$

where ε_s and ε_∞ are the static permittivity and relative dielectric permittivity at the high frequency limit, respectively. According to the equation, the plot of $\varepsilon' - \varepsilon''$ would be a single semicircle, and each semicircle means the occurrence of one Debye relaxation. Compared with the pure biocarbon holding one semicircle, each biocarbon-based composite displayed more than one semicircle, indicating the existence of multiple Debye relaxation processes as described above. The cole–cole curve of the pure biocarbon appeared as a long straight line in a low frequency range, indicating that conduction loss plays an important role in the pure carbon. Meanwhile, the biocarbon/NiCo composites presented two or more semicircles and one additional tail, suggesting the existence of polarization loss and conduction loss that cooperatively brought strong absorption.

3.3. Microwave absorption properties of biocarbon/NiCo composites

Fig. 7(a)–(d) reveals that the RL curves of the biocarbon/NiCo composites with different NiCo contents were depend-

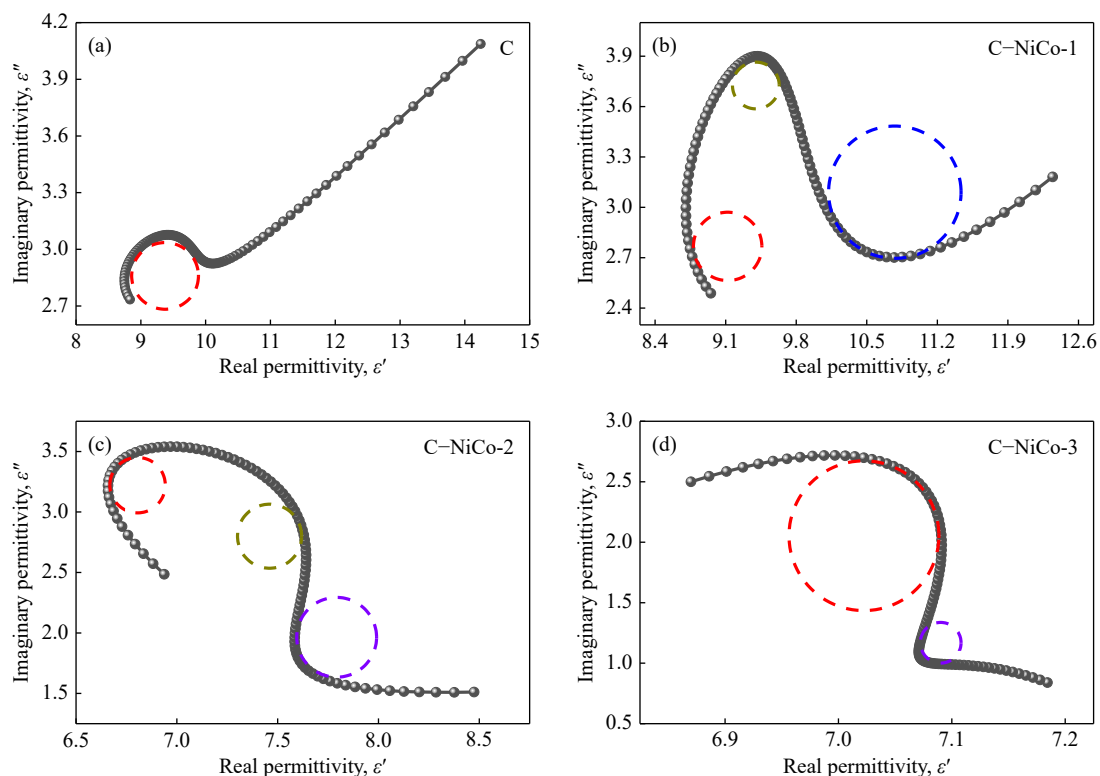


Fig. 6. Cole–cole plots of pure biocarbon and biocarbon/NiCo composites: (a) pure biocarbon, (b) C–NiCo-1, (c) C–NiCo-2, and (d) C–NiCo-3.

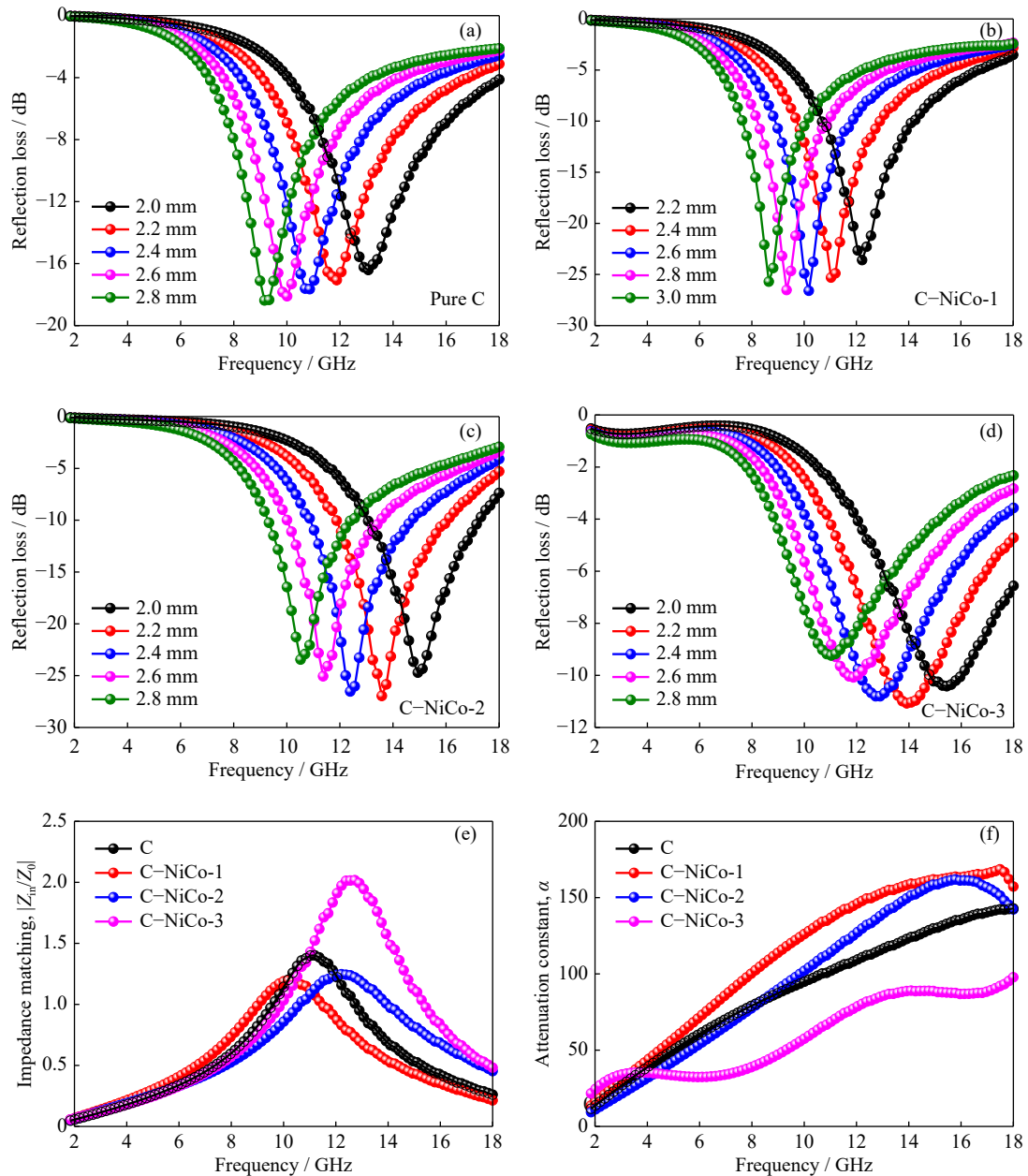


Fig. 7. RL values of biocarbon/NiCo composites: (a) pure biocarbon, (b) C-NiCo-1, (c) C-NiCo-2, and (d) C-NiCo-3. Impedance matching (2.2 mm) (e) and attenuation constant (f) of the four samples.

ent on the absorption thickness (2.0–3.0 mm) and frequency (2.0–18.0 GHz). RL is commonly calculated by transmission line theory shown in Eqs. (2) and (3) [14–15]:

$$RL = 20 \lg \left| \frac{Z_{in} - Z_0}{Z_{in} + Z_0} \right| \quad (2)$$

$$Z_{in} = Z_0 \sqrt{\frac{\mu_r}{\epsilon_r}} \tanh \left(j \frac{2\pi d f \sqrt{\mu_r \epsilon_r}}{c} \right) \quad (3)$$

where Z_{in} , Z_0 , c , f , d , μ_r , ϵ_r , and j denote the normalized input impedance, the impedance of air, the light speed in a vacuum, the frequency of incident EM waves, the thickness of absorbers, complex permeability, complex permittivity, and imaginary unit, respectively. For the pure biocarbon (Fig. 7(a)) of 2.8 mm thickness, the RL_{min} was -18.4 dB at 9.33 GHz. Owing to the addition of NiCo alloys, the C-NiCo-1 (Fig. 7(b)) and C-NiCo-2 (Fig. 7(c)) samples showed relat-

ively improved microwave absorption of -26.6 dB at 10.18 GHz of 2.6 mm and -27.0 dB at 13.58 GHz of 2.2 mm. Correspondingly, the EAB widths of the two biocarbon/NiCo materials were enhanced from 3.1 GHz (8.8–11.9 GHz) to 4.4 GHz (11.7–16.1 GHz). However, with the increase in NiCo content, the RL_{min} of the C-NiCo-3 sample (Fig. 7(d)) decreased to -11.1 dB at 13.92 GHz of 2.2 mm thickness, and the EAB was only 1.8 GHz (13.1–14.9 GHz). For the four samples, the excellent RL values shifted toward lower frequency with the increasing absorbing thickness due to the factor of the quarter-wavelength matching model. Compared with pure biocarbon, the biocarbon/NiCo composites had stronger microwave dissipation ability due to the improvement of magnetic loss capability and EM attenuation property [42–43]. However, a high NiCo content caused a poor microwave absorption performance due to impedance mis-

matching. The impedance matching ($|Z_{in}/Z_0|$) and attenuation constant (α) of the biocarbon/NiCo composites were calculated as shown in Fig. 7(e) and (f) to further investigate the EM absorbing property. Fig. 7(e) shows that the areas showing the $|Z_{in}/Z_0|$ values of C–NiCo-1 and C–NiCo-2 composites were close to 1, and those of the pure biocarbon and C–NiCo-3 composite were far away from 1. These results suggested that C–NiCo-1 and C–NiCo-2 possess good impedance matching, which prompts EM waves to enter the absorber. Similarly, the α values (Fig. 7(f)) of the four samples showed the same trend as the impedance matching, suggesting the good EM wave attenuation capability of C–NiCo-1 and C–NiCo-2.

An appropriate impedance match obtained by tuning the component, thickness, and frequency of the promising absorber is pivotal in the absorbing properties. The matched thickness versus frequency was simulated using the quarter-wavelength model in the following formula:

$$d = \frac{n\lambda}{4} = \frac{n\lambda_0}{4\sqrt{|\mu_r|\epsilon_r|}} \quad (n = 1, 3, 5, 7, 9, \dots) \quad (4)$$

where λ and λ_0 are the wavelengths of the incident EM wave inside the material and in the vacuum, respectively. The minimal RL values shifted to the low frequency range when the simulated thickness was increased, and this finding agreed

with the theory of the $\lambda/4$ matching model [43].

Table 1 presents the comparison of microwave capability of various carbon materials [10,44–54]. The NiCo/biocarbon composites exhibited competitive microwave absorption properties. The possible mechanism of the microwave absorption of porous biocarbon/NiCo composites was explained in the following aspects. First, the biocarbon and magnetic components can induce interfacial polarization loss and conductive loss, thus creating a high dielectric loss [55]. Second, the magnetic nature of NiCo alloys provides a good magnetic loss ability through natural resonance and eddy current effect [56]. Third, the NiCo alloy could transform EM energy into heat because of magnetic loss, thus leading to magnetic coupling interactions occurring in adjacent magnetic nanoparticles; the density of the magnetic flux line irradiated out from the shell surface could be slightly deformed and augmented around the NiCo, thus transferring the biocarbon surface to a “magnetism-rich” configuration [8]. Finally, the porous structure of straw-derived biochar would cause the scattering of EM waves in the absorber and dissipate the incident EM wave as far as possible [57]. Thus, the combination of dielectric loss and magnetic loss can provide a good impedance match, thereby endowing the biocarbon/NiCo composites with a high-efficiency absorbing ability.

Table 1. Comparison of microwave capability among various carbon materials

Sample	Filler content / wt%	Matrix	RL _{min} / dB	Thickness / mm	Frequency range (RL < -10 dB) / GHz	Ref.
Co/CoO@C	50	Paraffin	-45.0	6.0	4.4–18.0	[44]
Co/C	30	Paraffin	-15.7	1.7	12.3–17.7	[45]
Co/CNT	50	Paraffin	-16.0	2.0	5.1–8.8	[46]
MWCNTs/Co	60	Epoxy resin	-37.0	5.25	6.7–18.0	[47]
Co/MOF-derived C	60	paraffin	-25.0	1.9	12.3–18.0	[48]
Fe–Co/ MOF-derived C	50	Paraffin	-21.7	1.2	12.2–18.0	[49]
FeNi/C nanofibers	30	Paraffin	-24.8	2.7	12.8–17.2	[50]
NiCo/C	25	Paraffin	-36.5	2.2	14.4–18.0	[51]
Fe/CNT	17	Epoxy	-25.0	1.2	2.0–18.0	[10]
Co _{0.2} Ni _{0.8} Fe ₂ O ₄ /RGO	60	Paraffin	-19.5	2.0	10.5–12.4	[52]
Ni/C	30	Paraffin	-20.5	1.7	11.8–18.0	[53]
Co–Ni/C	30	Paraffin	-34.3	3.3	13.8–18.0	[53]
Fe–Ni/C	30	Paraffin	-42.3	5.7	15.2–18.0	[53]
Ni/carbon spheres	40	paraffin	-20.3	9.0	12.5–15.5	[54]
NiCo/biocarbon	30	Paraffin	-27.0	2.2	11.7–16.1	This work

4. Conclusion

Porous structured biocarbon/NiCo materials were fabricated through high-temperature reduction and subsequent hydrothermal reaction. The magnetic NiCo alloys enhanced the dielectric loss through intense interfacial polarization. The formation of conductive networks between the porous biocarbon and NiCo alloys induced conductive loss. An exceptional RL_{min} of -27.0 dB at 2.2 mm thickness and an EAB width of 4.4 GHz (11.7–16.1 GHz) were achieved. We believe that the construction of magnetic biocarbon composites

will be useful in designing a high-performance absorbing material.

Acknowledgements

This work was financially supported by the National Natural Science Foundation of China (No. U2004177), the Henan Province Science and Technology Research and Development Project in 2020, China (No. 202300410491), and the Key Scientific Research Projects of Provincial Universities in 2021, China (No. 21A430045).

Conflict of Interest

The authors declare no conflict of interest.

References

- [1] P. Zhou, J.H. Chen, M. Liu, P. Jiang, B. Li, and X.M. Hou, Microwave absorption properties of SiC@SiO₂@Fe₃O₄ hybrids in the 2–18 GHz range, *Int. J. Miner. Metall. Mater.*, 24(2017), No. 7, p. 804.
- [2] Y.F. Zhang, Z. Ji, K. Chen, C.C. Jia, S.W. Yang, and M.Y. Wang, Preparation and radar-absorbing properties of Al₂O₃/TiO₂/Fe₂O₃/Yb₂O₃ composite powder, *Int. J. Miner. Metall. Mater.*, 24(2017), No. 2, p. 216.
- [3] H.L. Lv, Z.H. Yang, B. Liu, et al., A flexible electromagnetic wave-electricity harvester, *Nat. Commun.*, 12(2021), No. 1, p. 1.
- [4] Y. Li, Y.C. Qing, Y.F. Zhou, et al., Unique nanoporous structure derived from Co₃O₄-C and Co/CoO-C composites towards the ultra-strong electromagnetic absorption, *Composites Part B*, 213(2021), art. No. 108731.
- [5] B. Zhao, X.Q. Guo, W.Y. Zhao, et al., Yolk-shell Ni@SnO₂ composites with a designable interspace to improve the electromagnetic wave absorption properties, *ACS Appl. Mater. Interfaces*, 8(2016), No. 42, p. 28917.
- [6] Q.H. Liu, Q. Cao, H. Bi, et al., CoNi@SiO₂@TiO₂ and CoNi@Air@TiO₂ microspheres with strong wideband microwave absorption, *Adv. Mater.*, 28(2016), No. 3, p. 486.
- [7] J.W. Liu, R.C. Che, H.J. Chen, et al., Microwave absorption enhancement of multifunctional composite microspheres with spinel Fe₃O₄ cores and anatase TiO₂ shells, *Small*, 8(2012), No. 8, p. 1214.
- [8] B. Zhao, Y. Li, Q.W. Zeng, et al., Galvanic replacement reaction involving core-shell magnetic chains and orientation-tunable microwave absorption properties, *Small*, 16(2020), No. 40, art. No. 2003502.
- [9] B. Zhao, X.Q. Guo, W.Y. Zhao, et al., Facile synthesis of yolk-shell Ni@void@SnO₂(Ni₃Sn₂) ternary composites via galvanic replacement/Kirkendall effect and their enhanced microwave absorption properties, *Nano Res.*, 10(2017), No. 1, p. 331.
- [10] R.C. Che, L.M. Peng, X.F. Duan, Q. Chen, and X.L. Liang, Microwave absorption enhancement and complex permittivity and permeability of Fe encapsulated within carbon nanotubes, *Adv. Mater.*, 16(2004), No. 5, p. 401.
- [11] B. Zhao, Y. Li, H.Y. Ji, et al., Lightweight graphene aerogels by decoration of 1D CoNi chains and CNTs to achieve ultra-wide microwave absorption, *Carbon*, 176(2021), p. 411.
- [12] N. Zhang, Y. Huang, M.Y. Wang, X.D. Liu, and M. Zong, Design and microwave absorption properties of thistle-like CoNi enveloped in dielectric Ag decorated graphene composites, *J. Colloid Interface Sci.*, 534(2019), p. 110.
- [13] H. Wang, Y.Y. Dai, W.J. Gong, et al., Broadband microwave absorption of CoNi@C nanocapsules enhanced by dual dielectric relaxation and multiple magnetic resonances, *Appl. Phys. Lett.*, 102(2013), No. 22, art. No. 223113.
- [14] Z.C. Lou, Q.Y. Wang, U.I. Kara, et al., Biomass-derived carbon heterostructures enable environmentally adaptive wide-band electromagnetic wave absorbers, *Nano Micro Lett.*, 14(2021), No. 1, p. 1.
- [15] Y. Liu, Z.R. Jia, Q.Q. Zhan, Y.H. Dong, Q.M. Xu, and G.L. Wu, Magnetic manganese-based composites with multiple loss mechanisms towards broadband absorption, *Nano Res.*, 15(2022), No. 6, p. 5590.
- [16] Y. Wu, R.W. Shu, Z.Y. Li, et al., Design and electromagnetic wave absorption properties of reduced graphene oxide/multi-walled carbon nanotubes/nickel ferrite ternary nanocomposites, *J. Alloys Compd.*, 784(2019), p. 887.
- [17] H. Sun, R.C. Che, X. You, et al., Cross-stacking aligned carbon-nanotube films to tune microwave absorption frequencies and increase absorption intensities, *Adv. Mater.*, 26(2014), No. 48, p. 8120.
- [18] B. Zhao, J.S. Deng, C.X. Zhao, et al., Achieving wideband microwave absorption properties in PVDF nanocomposite foams with an ultra-low MWCNT content by introducing a microcellular structure, *J. Mater. Chem. C*, 8(2020), No. 1, p. 58.
- [19] T.S. Liu, N. Liu, S.R. Zhai, et al., Tailor-made core/shell/shell-like Fe₃O₄@SiO₂@PPy composites with prominent microwave absorption performance, *J. Alloys Compd.*, 779(2019), p. 831.
- [20] X.Y. Wu, B.Y. Han, H.B. Zhang, et al., Compressible, durable and conductive polydimethylsiloxane-coated MXene foams for high-performance electromagnetic interference shielding, *Chem. Eng. J.*, 381(2020), art. No. 122622.
- [21] X.L. Cao, Z.R. Jia, D.Q. Hu, and G.L. Wu, Synergistic construction of three-dimensional conductive network and double heterointerface polarization via magnetic FeNi for broadband microwave absorption, *Adv. Compos. Hybrid Mater.*, 5(2022), No. 2, p. 1030.
- [22] M.A. Aslam, W. Ding, S. ur Rehman, et al., Low cost 3D bio-carbon foams obtained from wheat straw with broadened bandwidth electromagnetic wave absorption performance, *Appl. Surf. Sci.*, 543(2021), art. No. 148785.
- [23] Y.Y. Wang, Z.H. Zhou, J.L. Zhu, et al., Low-temperature carbonized carbon nanotube/cellulose aerogel for efficient microwave absorption, *Composites Part B*, 220(2021), art. No. 108985.
- [24] H.Q. Zhao, Y. Cheng, H.L. Lv, B.S. Zhang, G. Ji, and Y.W. Du, Achieving sustainable ultralight electromagnetic absorber from flour by turning surface morphology of nanoporous carbon, *ACS Sustain. Chem. Eng.*, 6(2018), No. 11, p. 15850.
- [25] X.X. Sun, M.L. Yang, S. Yang, et al., Ultrabroad band microwave absorption of carbonized waxberry with hierarchical structure, *Small*, 15(2019), No. 43, art. No. 1902974.
- [26] G.J. Gou, F.B. Meng, H.G. Wang, M. Jiang, W. Wei, and Z.W. Zhou, Wheat straw-derived magnetic carbon foams: In-situ preparation and tunable high-performance microwave absorption, *Nano Res.*, 12(2019), No. 6, p. 1423.
- [27] H.Q. Zhao, Y. Cheng, J.N. Ma, Y.N. Zhang, G.B. Ji, and Y.W. Du, A sustainable route from biomass cotton to construct lightweight and high-performance microwave absorber, *Chem. Eng. J.*, 339(2018), p. 432.
- [28] H.Q. Zhao, Y. Cheng, H.L. Lv, G.B. Ji, and Y.W. Du, A novel hierarchically porous magnetic carbon derived from biomass for strong lightweight microwave absorption, *Carbon*, 142(2019), p. 245.
- [29] P.F. Yin, L.M. Zhang, Y.Y. Jiang, et al., Recycling of waste straw in sorghum for preparation of biochar/(Fe,Ni) hybrid aimed at significant electromagnetic absorbing of low-frequency band, *J. Mater. Res. Technol.*, 9(2020), No. 6, p. 14212.
- [30] J. Cui, X.H. Wang, L. Huang, C.W. Zhang, Y. Yuan, and Y.B. Li, Environmentally friendly bark-derived Co-Doped porous carbon composites for microwave absorption, *Carbon*, 187(2022), p. 115.
- [31] B. Zhao, G. Shao, B.B. Fan, W.Y. Zhao, Y.J. Xie, and R. Zhang, Synthesis of flower-like CuS hollow microspheres based on nanoflakes self-assembly and their microwave absorption properties, *J. Mater. Chem. A*, 3(2015), No. 19, p. 10345.
- [32] J. Feng, F.Z. Pu, Z.X. Li, X.H. Li, X.Y. Hu, and J.T. Bai, Interfacial interactions and synergistic effect of CoNi nanocrystals and nitrogen-doped graphene in a composite microwave absorber, *Carbon*, 104(2016), p. 214.
- [33] L.L. Liang, Z.Q. Zhang, F. Song, et al., Ultralight, flexible carbon hybrid aerogels from bacterial cellulose for strong mi-

- crowave absorption, *Carbon*, 162(2020), p. 283.
- [34] H.L. Lv, Z.H. Yang, H.B. Xu, L.Y. Wang, and R.B. Wu, An electrical switch-driven flexible electromagnetic absorber, *Adv. Funct. Mater.*, 30(2020), No. 4, art. No. 1907251.
- [35] Y.C. Qing, Y. Li, W. Li, and H.Y. Yao, Ti^{3+} self-doped dark TiO_2 nanoparticles with tunable and unique dielectric properties for electromagnetic applications, *J. Mater. Chem. C*, 9(2021), No. 4, p. 1205.
- [36] X.F. Zhang, P.F. Guan, and X.L. Dong, Transform between the permeability and permittivity in the close-packed Ni nanoparticles, *Appl. Phys. Lett.*, 97(2010), No. 3, art. No. 033107.
- [37] Z.X. Yu, N. Zhang, Z.P. Yao, X.J. Han, and Z.H. Jiang, Synthesis of hierarchical dendritic micro-nano structure $\text{Co}_x\text{Fe}_{1-x}$ alloy with tunable electromagnetic absorption performance, *J. Mater. Chem. A*, 1(2013), No. 40, p. 12462.
- [38] Z.C. Wu, K. Pei, L.S. Xing, X.F. Yu, W.B. You, and R.C. Che, Enhanced microwave absorption performance from magnetic coupling of magnetic nanoparticles suspended within hierarchically tubular composite, *Adv. Funct. Mater.*, 29(2019), No. 28, art. No. 1901448.
- [39] R. Qiang, Y.C. Du, H.T. Zhao, *et al.*, Metal organic framework-derived Fe/C nanocubes toward efficient microwave absorption, *J. Mater. Chem. A*, 3(2015), No. 25, p. 13426.
- [40] X. Wen, L.Z. Hou, L.W. Deng, D.T. Kuang, H. Luo, and S.L. Wang, Facile fabrication of extremely small CoNi/C core/shell nanoparticles for efficient microwave absorber, *Nano*, 14(2019), No. 7, art. No. 1950090.
- [41] H.L. Lv, Z.H. Yang, S.J.H. Ong, *et al.*, A flexible microwave shield with tunable frequency-transmission and electromagnetic compatibility, *Adv. Funct. Mater.*, 29(2019), No. 14, art. No. 1900163.
- [42] C. Zhang, C. Long, S. Yin, *et al.*, Graphene-based anisotropic polarization meta-filter, *Mater. Des.*, 206(2021), art. No. 109768.
- [43] Z.C. Lou, Q.Y. Wang, Y. Zhang, *et al.*, *In-situ* formation of low-dimensional, magnetic core-shell nanocrystal for electromagnetic dissipation, *Composites Part B*, 214(2021), art. No. 108744.
- [44] M.L. Yang, Y. Yuan, W.L. Yin, *et al.*, Co/CoO@C nanocomposites with a hierarchical bowknot-like nanostructure for high performance broadband electromagnetic wave absorption, *Appl. Surf. Sci.*, 469(2019), p. 607.
- [45] B.Y. Zhu, P. Miao, J. Kong, X.L. Zhang, G.Y. Wang, and K.J. Chen, Co/C composite derived from a newly constructed metal-organic framework for effective microwave absorption, *Cryst. Growth Des.*, 19(2019), No. 3, p. 1518.
- [46] Z. Zheng, B. Xu, L. Huang, L. He, and X.M. Ni, Novel composite of Co/carbon nanotubes: Synthesis, magnetism and microwave absorption properties, *Solid State Sci.*, 10(2008), No. 3, p. 316.
- [47] F.S. Wen, F. Zhang, and Z.Y. Liu, Investigation on microwave absorption properties for multiwalled carbon nanotubes/Fe/Co/Ni nanopowders as lightweight absorbers, *J. Phys. Chem. C*, 115(2011), No. 29, p. 14025.
- [48] W. Liu, L. Liu, Z.H. Yang, J.J. Xu, Y.L. Hou, and G.B. Ji, A versatile route toward the electromagnetic functionalization of metal-organic framework-derived three-dimensional nanoporous carbon composites, *ACS Appl. Mater. Interfaces*, 10(2018), No. 10, p. 8965.
- [49] X.M. Zhang, G.B. Ji, W. Liu, *et al.*, Thermal conversion of an Fe_3O_4 @metal-organic framework: A new method for an efficient Fe-Co/nanoporous carbon microwave absorbing material, *Nanoscale*, 7(2015), No. 30, p. 12932.
- [50] J. Lv, X.H. Liang, G.B. Ji, B. Quan, W. Liu, and Y.W. Du, Structural and carbonized design of 1D FeNi/C nanofibers with conductive network to optimize electromagnetic parameters and absorption abilities, *ACS Sustainable Chem. Eng.*, 6(2018), No. 6, p. 7239.
- [51] H.F. Qiu, X.Y. Zhu, P. Chen, J.L. Liu, and X.L. Zhu, Self-etching template method to synthesize hollow dodecahedral carbon capsules embedded with Ni-Co alloy for high-performance electromagnetic microwave absorption, *Compos. Commun.*, 20(2020), art. No. 100354.
- [52] A. Das, P. Negi, S.K. Joshi, and A. Kumar, Enhanced microwave absorption properties of Co and Ni co-doped iron (II, III)/reduced graphene oxide composites at X-band frequency, *J. Mater. Sci. Mater. Electron.*, 30(2019), No. 21, p. 19325.
- [53] X.L. Wu, K. Liu, J.W. Ding, *et al.*, Construction of Ni-based alloys decorated sucrose-derived carbon hybrid towards: Effective microwave absorption application, *Adv. Compos. Hybrid Mater.*, 5(2022), 3, p. 2260.
- [54] Z.B. Su, J. Tao, J.Y. Xiang, Y. Zhang, C. Su, and F.S. Wen, Structure evolution and microwave absorption properties of nickel nanoparticles incorporated carbon spheres, *Mater. Res. Bull.*, 84(2016), p. 445.
- [55] H.L. Lv, Z.H. Yang, P.L. Wang, *et al.*, A voltage-boosting strategy enabling a low-frequency, flexible electromagnetic wave absorption device, *Adv. Mater.*, 30(2018), No. 15, art. No. 1706343.
- [56] Y. Li, Y.C. Qing, B. Zhao, *et al.*, Tunable magnetic coupling and dipole polarization of core-shell Magnéli Ti_4O_7 ceramic/magnetic metal possessing broadband microwave absorption properties, *Ceram. Int.*, 47(2021), No. 23, p. 33373.
- [57] H. Du, Q.P. Zhang, B. Zhao, *et al.*, Novel hierarchical structure of $\text{MoS}_2/\text{TiO}_2/\text{Ti}_3\text{C}_2\text{T}_x$ composites for dramatically enhanced electromagnetic absorbing properties, *J. Adv. Ceram.*, 10(2021), No. 5, p. 1042.